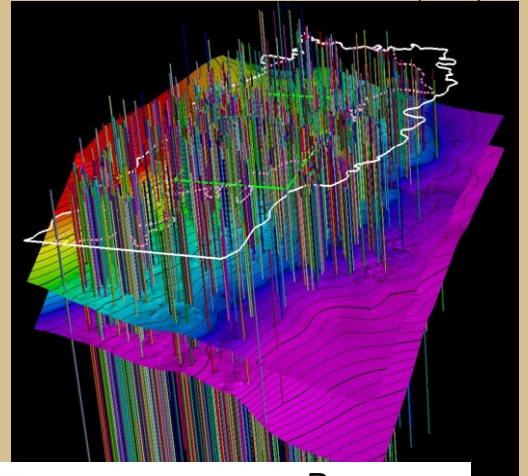
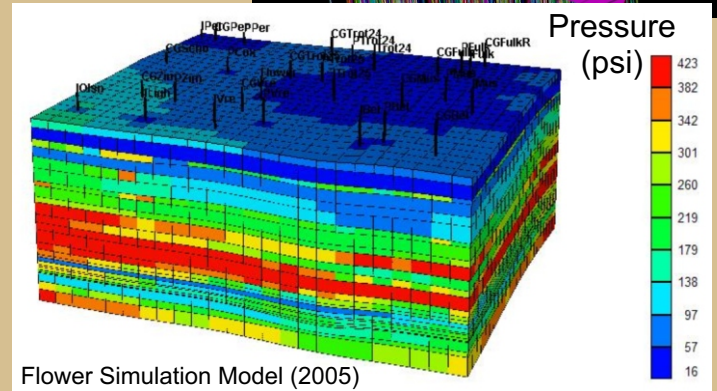
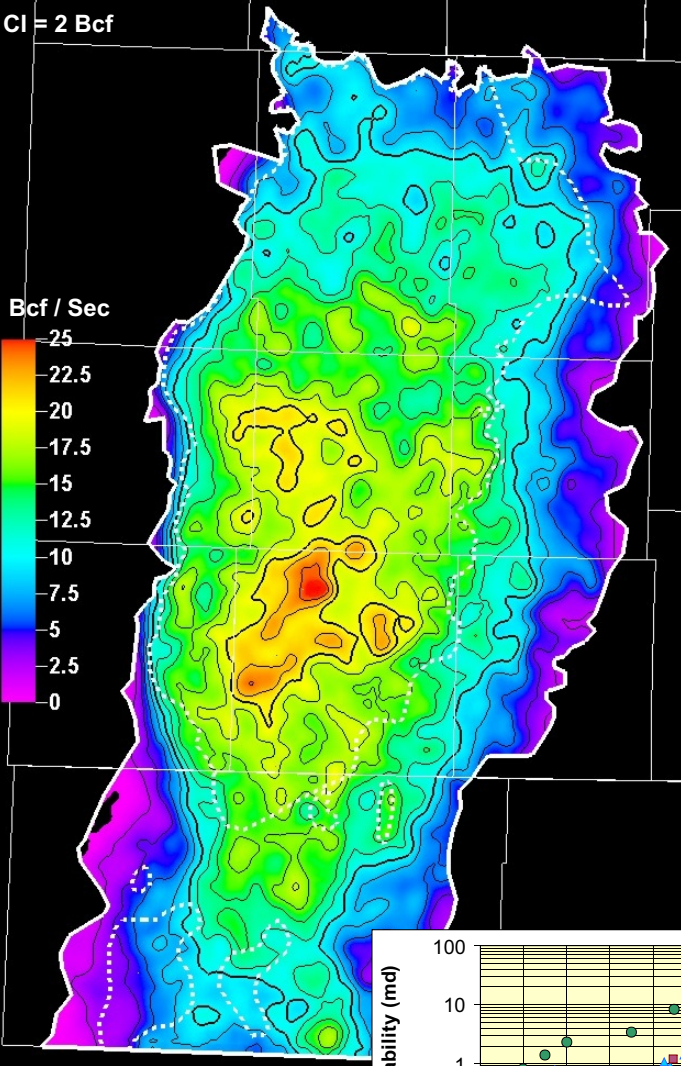


# Hugoton Asset Management Project (HAMP)

Model "Node" Wells (1600)

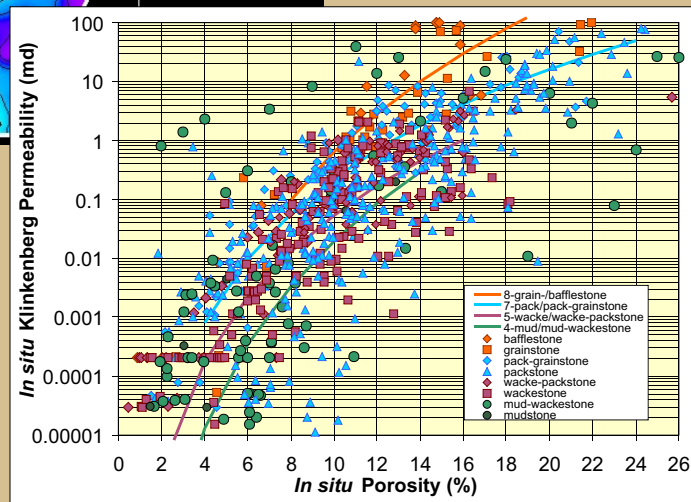


Wolfcampian Volumetric OGIP (BCF/Sec)



# Hugoton Geomodel Final Report

Martin K. Dubois  
 Alan P. Byrnes  
 Saibal Bhattacharya  
 Geoffrey C. Bohling  
 John H. Doveton  
 Robert E. Barba



Permeability-Porosity Trend by Lithofacies



Phylloid Algal Mound Facies

# **HUGOTON ASSET MANAGEMENT PROJECT (HAMP): HUGOTON GEOMODEL FINAL REPORT**

*Martin K. Dubois, Alan P. Byrnes, Saibal Bhattacharya, Geoffrey C. Bohling, John H. Doveton, and Robert E. Barba*

## **DISCLAIMER**

Results and conclusions in reports or papers related to the Hugoton Asset Management Project are based on objective scientific investigation and observations by Kansas Geological Survey (KGS) staff and consultants contracted by the KGS, and are only attributed to the authors. This study was made possible by contributions of data and funding by ten industry partners, however, the support of industry partners should not imply that they are in agreement with results and conclusions. The Kansas Geological Survey compiled this publication according to specific standards, using what is thought be the most reliable information available. The Kansas Geological Survey does not guarantee freedom from errors or inaccuracies and disclaims any legal responsibility or liability for interpretations made from the publication or decision based thereon.

## **ACKNOWLEDGEMENTS**

We are grateful for the support from partners in the Hugoton Asset Management Project (HAMP) including Anadarko Petroleum Corporation, BP America Production Company, ConocoPhillips Company, Cimarex Energy Company, E.O.G. Resources Inc., ExxonMobil Production Company, Medicine Bow Energy Corporation (now El Paso Exploration & Production), Osborn Heirs Company, OXY USA, Inc., and Pioneer Natural Resources USA, Inc.; and from the Kansas Geological Survey. The comprehensive field-wide study would not have been possible without pooling of previously proprietary geologic and engineering data by industry partners. A prior study, the Hugoton Project, directed by Timothy Carr, provided data critical for building the basic geologic framework for HAMP. We greatly appreciate Marla Adkins-Heljeson's editorial review of the complete document. We thank Raymond Sorenson for insightful discussions over the years, Shane Seals for work on earlier models, and geoPlus Corporation and Schlumberger for providing software.

## **INDUSTRY PARTICIPANTS**

Anadarko Petroleum Corporation  
BP America Production Company  
ConocoPhillips Company  
Cimarex Energy Company  
E.O.G. Resources Inc.  
ExxonMobil Production Company  
Medicine Bow Energy Corporation (now El Paso Exploration & Production)  
Osborn Heirs Company  
OXY USA, Inc.  
Pioneer Natural Resources USA, Inc.

## TECHNICAL GROUP

*Successful completion of the Hugoton Asset Management Project and its multi-iteration model building strategy was possible only through close and ongoing integration of work by members of the multi-discipline technical group at the Kansas Geological Survey and consultants over a 2-1/2 year period.*

### *Kansas Geological Survey*

Martin Dubois	Manager, sedimentology, static model
Timothy Carr	Co-manager (Deep Pools)
Alan Byrnes	Core petrophysics
Geoffrey Bohling	Geostatistics, programming, model
Saibal Bhattacharya	Reservoir engineering, simulation
John Doveton	Log petrophysics
John Victorine	Java programmer
Ken Stalder	Web site
Melissa Moore	Database management
Nathan Winters	Graduate student assistant

### *Consultants*

Robert Barba	Engineer, fracture modeling
Rick Brownrigg	Computer engineer, P/T visualization tool
Paul Gerlach	Geologist, Oklahoma Panhandle
David Hamilton	SCM, Petrel modeler
David Morgan	SCM, Petrel modeler

## ***Table of Contents***

Disclaimer .....	ii
Acknowledgements .....	ii
Industry Participants .....	ii
Technical Group.....	iii
Table of Contents .....	iv
List of Tables .....	vi
List of Figures .....	viii
List of Appendices .....	xvii
<b>Chapter 1: Introduction, <i>Martin K. Dubois and Alan P. Byrnes</i></b> .....	1-1
<b>Chapter 2: Geologic Setting, <i>Martin K. Dubois</i></b> .....	2-1
<b>Chapter 3: Depositional Model, <i>Martin K. Dubois</i></b> .....	3-1
<b>Chapter 4: Reservoir Characterization, <i>Alan P. Byrnes, Martin K. Dubois,</i></b> <i>and John H. Doveton</i> .....	4-1
4.1: Lithofacies classification, <i>Martin K. Dubois and Alan P. Byrnes</i> .....	4-1
4.2: Core Petrophysics, <i>Alan P. Byrnes</i> .....	4-13
4.3: Wireline Log Petrophysics, <i>John H. Doveton</i> .....	4-120
<b>Chapter 5: Technology to Manage Large Digital Datasets</b> .....	5-1
<i>Geoffrey C. Bohling</i>	
<b>Chapter 6: Static Reservoir Model, <i>Martin K. Dubois, Geoffrey C. Bohling,</i></b> <i>and Alan P. Byrnes</i> .....	6-1
6.1: Workflow, <i>Martin K. Dubois and Alan P. Byrnes</i> .....	6-3
6.2: Stuctural/Stratigraphic Grid Model, <i>Martin K. Dubois</i> .....	6-4
6.3 Lithofacies Estimation at Well- to Model-Scale,.....	6-5
<i>Geoffrey C. Bohling and Martin K. Dubois</i>	
6.4 Lithofacies Distribution in the Static Model, <i>Martin K. Dubois</i> .....	6-11
6.5 Porosity Model, <i>Martin K. Dubois and Geoffrey C. Bohling</i> .....	6-15
6.6 Petrophysical Model, <i>Alan P. Byrnes and Martin K. Dubois</i> .....	6-16
<b>Chapter 7: Water Saturations and Free-Water Level, <i>Alan P. Byrnes and</i></b> <i>Martin K. Dubois</i> .....	7-1
7.1 Core and Log Petrophysics, <i>Alan P. Byrnes</i> .....	7-2

7.2 Resolving Free Water Level Geometry, <i>Martin K. Dubois</i> .....	7-7
7.3 Sensitivity of OGIP to Capillary Pressure and Free Water Level, .....	7-10
<i>Alan P. Byrnes and Martin K. Dubois</i>	
<b>Chapter 8: Reservoir Communication, <i>Alan P. Byrnes, Martin K. Dubois, Saibal</i></b>	
<i>Bhattacharya, and Robert E. Barba</i> .....	
	8-1
8.1 Core- to Well-Scaling, <i>Alan P. Byrnes</i> .....	8-1
8.2 Potential Influence of Thin High-Permeability Beds and Crossflow .....	8-15
<i>Alan P. Byrnes</i>	
8.3 Communication between Chase and Council Grove, <i>Martin K. Dubois</i> .....	8-27
8.4 Differential Depletion of Reservoir Pressure – Simulation Studies .....	8-42
<i>Saibal Bhattacharya</i>	
8.5 Hydraulic Fractures, <i>Robert E. Barba and Martin K. Dubois</i> .....	8-50
<b>Chapter 9: Reservoir Simulation, <i>Saibal Bhattacharya, Martin K. Dubois</i></b>	
<i>and Alan P. Byrnes</i> .....	
	9-1
9.1 Reservoir Simulation Overview.....	9-1
<i>Saibal Bhattacharya, Martin K. Dubois and Alan P. Byrnes</i>	
9.2 Single-Section Simulation – Alexander D2.....	9-16
<i>Saibal Bhattacharya, Martin K. Dubois and Alan P. Byrnes</i>	
9.3 Multi-Section Simulation – Flower Area.....	9-50
<i>Saibal Bhattacharya, Martin K. Dubois and Alan P. Byrnes</i>	
9.4 Multi-Section Simulation – Graskell Area .....	9-118
<i>Saibal Bhattacharya, Martin K. Dubois and Alan P. Byrnes</i>	
9.5 Multi-Section Simulation – Hoobler Area.....	9-175
<i>Saibal Bhattacharya, Martin K. Dubois and Alan P. Byrnes</i>	
9.6 Material-Balance Studies, <i>Saibal Bhattacharya</i> .....	9-235
9.6 Lessons Learned, <i>Saibal Bhattacharya</i> .....	9-260
<b>Chapter 10: Original and Remaining Gas in Place, <i>Martin K. Dubois</i></b> .....	10-1
10.1 OGIP in the Static Model.....	10-1
10.2 Remaining Gas in Hugoton and Panoma .....	10-16
<b>Chapter 11: Conclusions, <i>Martin K. Dubois, Alan P. Byrnes, and Saibal</i></b>	
<i>Bhattacharya</i> .....	
	11-1

## List of Tables

TABLE	PAGE
<b>Chapter 4: Reservoir Characterization</b>	
4.1.1 Digital lithofacies description system- 5 digit .....	4-5
4.1.2 Digital code for 11 lithofacies.....	4-6
4.1.3 Digital lithofacies description system- 12 digit .....	4-7
4.2.1 Core analysis database .....	A4.2.1
4.2.2 Summary statistics for grain density by group/member .....	4-41
4.2.3 Summary statistics for grain density by group/lithofacies.....	4-42
4.2.4 Summary statistics for porosity by group/lithofacies .....	4-43
4.2.5 Summary statistics for permeability by group/lithofacies .....	4-43
4.2.6 Equation parameters for predicting permeability by lithofacies.....	4-45
4.2.7 Interval-specific equation parameters for predicting permeability .....	4-45
4.2.8 Equation parameters for predicting capillary pressure by lithofacies.....	4-46
4.2.9 Capillary pressure database.....	A4.2.2
4.2.10 Relative permeability database .....	A4.2.3
4.2.11 Summary statistics of full-diameter $k_v/k_h$ ratio .....	4-47
<b>Chapter 6: Static Reservoir Model</b>	
6.1 Tops set for 25 formation/member level (1/2-cycle) intervals .....	6-23
6.2 Input files required for building cellular geomodel. ....	6-23
6.3 Variograms ranges for modeling lithofacies and porosity, Chase .....	6-24
6.4 Variograms ranges for modeling lithofacies and porosity, Council Grove ...	6-25
6.5 Relative distribution lithofacies in core, node wells and cellular model .....	6-26
<b>Chapter 7: Water Saturations and Free-Water Level</b>	
7.3.1 Differences in water saturation models for continental lithofacies .....	7-16
7.3.2 Differences in water saturation models for marine lithofacies .....	7-17
7.3.3 Differences in water saturation models for limestone lithofacies.....	7-18
7.3.4 Differences in water saturation models for dolomite lithofacies .....	7-19
7.3.5 Summary of depths with maximum Sw error for continental lithofacies.....	7-20
7.3.6 Summary of depths with maximum Sw error for marine lithofacies.....	7-21
7.3.7 Summary of depths with maximum Sw error for limestone lithofacies .....	7-22
7.3.8 Summary of depths with maximum Sw error for dolomite lithofacies .....	7-23
7.3.9 Comparison of OGIP by zone in three simulation models .....	7-24
<b>Chapter 8: Reservoir Communication</b>	
8.1.1 Equation parameters for predicting permeability by lithofacies.....	8-5
8.1.2 Comparison of measured and calculated permeability for layered core.....	8-6
8.3.1 Types of pressure data available in study area.....	8-33
8.3.2 Pressures by zone for two closely spaced wells.....	8-33
8.5.1 Poisson's ration by mineralogy.....	8-59
8.5.2 Rock mechanical facies classification .....	8-59
8.5.3 Chase model properties by layer.....	8-60

8.5.4	Chase model properties by layer – fluid loss .....	8-60
8.5.5	Chase model properties by layer – leak-off coefficients .....	8-61
8.5.6	Chase model treatment schedule assumptions .....	8-61
8.5.7	Chase & Council Grove model properties by layer .....	8-62
8.5.8	Chase & Council Grove model properties by layer – fluid loss .....	8-62
8.5.9	Chase & Council Grove model properties by layer – leak-off coefficients...	8-63
8.5.10	Chase & Council Grove model treatment schedule assumptions .....	8-63
8.5.11	Council Grove model properties by layer – fluid loss .....	8-64
8.5.12	Council Grove model properties by layer – leak-off coefficients.....	8-64
8.5.13	Council Grove model treatment schedule assumptions .....	8-65
8.5.14	Chase infill model properties by layer .....	8-66
8.5.15	Chase infill model properties by layer – fluid loss .....	8-66
8.5.16	Chase infill model properties by layer – leak-off coefficients.....	8-67
8.5.17	Chase infill model treatment schedule assumptions .....	8-67

***Chapter 9: Reservoir Simulation***

9.1.1	List of simulation studies in Hugoton-Panoma fields.....	9-6
9.1.2	Overall recovery efficiency in Flower, Graskell, and Hoobler.....	9-6
9.1.3	Relative-permeability tables for different rock-types .....	9-12
9.1.4	Relative-permeability tables for different rock-types .....	9-13

***Chapter 10: Original and Remaining Gas in Place***

10.1.1	Original gas in place for Grant in Stevens County, Kansas by zone .....	10-8
10.1.2	Comparison of OGIP and cumulative gas, Grant and Stevens counties.....	10-8
10.1.3	Production efficiency for the three multi-section simulation models.....	10-9
10.1.4	Comparison of OGIP and cumulative by county for Hugoton .....	10-9
10.1.5	Pore volume, hydrocarbon pore volume, and OGIP for Wolfcamp .....	10-10
10.2.1	Pressures and GIP for the Flower simulation model by zone.....	10-20
10.2.2	Zone pressures for Flower well and nearby replacement well .....	10-21
10.2.3	GIP and gas produced through time, 28-well, 9-unit Flower model .....	10-22
10.2.4	Pressures and GIP for the Hoobler simulation model by zone .....	10-23
10.2.5	Summary statistics for zone pressure tests in Hugoton .....	10-23

## *List of Figures*

FIGURE	PAGE
<b><i>Chapter 1: Introduction</i></b>	
1.1	Workflow for field-scale Hugoton model.....1-9
1.2	Regulatory boundaries for Permian (Wolfcampian) gas and oil fields.....1-10
1.3	Gas production from the Wolfcampian.....1-11
1.4	Stratigraphic column, Hugoton field area.....1-11
1.5	Formation- and member-level stratigraphy correlated to wireline well log ..1-12
<b><i>Chapter 2: Geologic Setting</i></b>	
2.1	Early Permian Paleogeography.....2-4
2.2	Distribution of major lithofacies in the Mid-Continent .....2-5
2.3	South-north cross section AA' through Anadarko basin .....2-6
2.4	Stratigraphic cross-section of the Chase and Council Grove.....2-7
2.5	Present day structure of top of Wolfcampian .....2-8
2.6	Isopach map of Wolfcampian .....2-9
<b><i>Chapter 3: Depositional Model</i></b>	
3.1	Distribution of major lithofacies, late Wolfcampian .....3-11
3.2	Isopach of Wolfcampian .....3-12
3.3	Updip limit of B2_LM and B3_LM and updip extent of fusulinid biofacies 3-13
3.4	Lithofacies in stratigraphic cross-sections across the Hugoton shelf .....3-14
3.5	Fusulinid biofacies in core slabs .....3-15
3.6	Idealized Chase and Council Grove Groups cycles.....3-16
3.7	Vertical histograms showing the average relative distribution of lithofacies 3-17
3.8	Chase and Council Grove depositional cycles and sequence stratigraphy ....3-18
3.9	Lithofacies trends through time .....3-19
3.10	Idealized depositional models for the Council Grove.....3-20
3.11	Idealized depositional models for the Chase .....3-21
<b><i>Chapter 4: Reservoir Characterization</i></b>	
4.1.1	Distribution of Hugoton cores .....4-7
4.1.2	Diagram of lithofacies optimization process .....4-7
4.1.3	Major lithofacies in Chase and Council Grove (L0-L5).....4-8
4.1.4	Major lithofacies in Chase and Council Grove (L6-L10).....4-10
4.1.5	Relative proportions of major lithofacies in core .....4-12
4.2.1	Locations of wells with core-analysis data .....4-48
4.2.2	Frequency distribution of lithofacies for core.....4-49
4.2.3	Frequency distribution of grain density for major lithofacies groups.....4-50
4.2.4	Frequency distribution of grain density for continental lithofacies .....4-51
4.2.5	Difference between Chase and Council Grove continental grain density ....4-51
4.2.6	Frequency distribution of grain density for marine lithofacies.....4-52
4.2.7	Difference between Chase and Council Grove marine grain density .....4-52
4.2.8	Frequency distribution of grain density for limestone lithofacies .....4-53

4.2.9	Difference between Chase and Council Grove limestone grain density.....	4-53
4.2.10	Frequency distribution of grain density for dolomite lithofacies.....	4-54
4.2.11	Difference between Chase and Council Grove dolomite grain density .....	4-54
4.2.12	Frequency distribution of <i>in situ</i> porosity.....	4-55
4.2.13	Crossplot of routine and <i>in situ</i> porosity.....	4-55
4.2.14	Frequency distribution of porosity for continental lithofacies.....	4-56
4.2.15	Difference between Chase and Council Grove continental porosity .....	4-56
4.2.16	Frequency distribution of porosity for marine lithofacies .....	4-57
4.2.17	Difference between Chase and Council Grove marine porosity.....	4-57
4.2.18	Frequency distribution of porosity for limestone lithofacies.....	4-58
4.2.19	Difference between Chase and Council Grove limestone porosity .....	4-58
4.2.20	Frequency distribution of porosity for dolomite lithofacies .....	4-59
4.2.21	Difference between Chase and Council Grove dolomite porosity.....	4-59
4.2.22	Frequency distribution of plug and full-diameter permeability .....	4-60
4.2.23	Crossplot of routine-air permeability and porosity .....	4-61
4.2.24	Crossplot of <i>in situ</i> Klinkenberg and <i>in situ</i> air permeability .....	4-62
4.2.25	Crossplot of <i>in situ</i> Klinkenberg and routine Klinkenberg permeability.....	4-63
4.2.26	Crossplot of <i>in situ</i> Klinkenberg and routine air permeability .....	4-64
4.2.27	Crossplot of <i>in situ</i> Klinkenberg and routine air permeability other rocks....	4-65
4.2.28	Crossplot of pore-throat diameter and permeability .....	4-66
4.2.29	Frequency distribution of permeability for Chase and Council Grove.....	4-67
4.2.30	Frequency distribution of permeability for continental lithofacies.....	4-68
4.2.31	Difference between Chase and Council Grove continental permeability .....	4-68
4.2.32	Frequency distribution of permeability for marine lithofacies .....	4-69
4.2.32	Difference between Chase and Council Grove marine permeability.....	4-69
4.2.33	Frequency distribution of permeability for limestone lithofacies.....	4-70
4.2.34	Difference between Chase and Council Grove limestone permeability .....	4-70
4.2.35	Frequency distribution of permeability for dolomite lithofacies .....	4-71
4.2.36	Difference between Chase and Council Grove dolomite permeability .....	4-71
4.2.37	Crossplot of <i>in situ</i> Klinkenberg permeability and <i>in situ</i> porosity .....	4-72
4.2.38	Crossplot of <i>in situ</i> permeability and porosity for L0 lithofacies .....	4-73
4.2.39	Crossplot of <i>in situ</i> permeability and porosity for L1 lithofacies .....	4-73
4.2.40	Crossplot of <i>in situ</i> permeability and porosity for L2 lithofacies .....	4-74
4.2.41	Crossplot of <i>in situ</i> permeability and porosity for L3 lithofacies .....	4-74
4.2.42	Crossplot of <i>in situ</i> permeability and porosity for L4 lithofacies .....	4-75
4.2.43	Crossplot of <i>in situ</i> permeability and porosity for L5 lithofacies .....	4-75
4.2.44	Crossplot of <i>in situ</i> permeability and porosity for L6 lithofacies .....	4-76
4.2.45	Crossplot of <i>in situ</i> permeability and porosity for L7 lithofacies .....	4-77
4.2.46	Crossplot of <i>in situ</i> permeability and porosity for L8 lithofacies .....	4-78
4.2.47	Crossplot of <i>in situ</i> permeability and porosity for L9 lithofacies .....	4-78
4.2.48	Crossplot of <i>in situ</i> permeability and porosity for L10 lithofacies .....	4-79
4.2.49	Crossplot of <i>in situ</i> permeability and porosity for continental lithofacies.....	4-80
4.2.50	Crossplot of <i>in situ</i> permeability and porosity for marine lithofacies .....	4-81
4.2.51	Crossplot of <i>in situ</i> permeability and porosity for limestone lithofacies .....	4-82
4.2.52	Crossplot of <i>in situ</i> permeability and porosity for L10 lithofacies .....	4-83
4.2.53	Selected capillary pressure curves for different permeability.....	4-84

4.2.54	Crossplot of log threshold-entry height and permeability .....	4-85
4.2.55	Crossplot of log threshold-entry height and log porosity .....	4-85
4.2.56	Crossplot of log threshold-entry height and porosity .....	4-86
4.2.57	Crossplot of threshold-entry height and porosity-continental lithofacies.....	4-87
4.2.58	Crossplot of threshold-entry height and porosity-marine lithofacies .....	4-88
4.2.59	Crossplot of threshold-entry height and porosity-limestone lithofacies .....	4-89
4.2.60	Crossplot of threshold-entry height and porosity-dolomite lithofacies .....	4-90
4.2.61	Histogram of correlation coefficients of height fractal slope equations .....	4-91
4.2.62	Crossplot of height fractal slope and porosity .....	4-92
4.2.63	Crossplot of height fractal slope and porosity for continental lithofacies .....	4-93
4.2.64	Crossplot of height fractal slope and porosity for marine lithofacies .....	4-94
4.2.65	Crossplot of height fractal slope and porosity for limestone lithofacies .....	4-95
4.2.66	Crossplot of height fractal slope and porosity for dolomite lithofacies.....	4-96
4.2.67	Model $H_{afwl}$ versus $S_w$ curves for L0 lithofacies .....	4-97
4.2.68	Model $H_{afwl}$ versus $S_w$ curves for L1 lithofacies .....	4-97
4.2.69	Model $H_{afwl}$ versus $S_w$ curves for L2 lithofacies .....	4-98
4.2.70	Model $H_{afwl}$ versus $S_w$ curves for L3 lithofacies .....	4-99
4.2.71	Model $H_{afwl}$ versus $S_w$ curves for L10 lithofacies .....	4-99
4.2.72	Model $H_{afwl}$ versus $S_w$ curves for L4 lithofacies .....	4-100
4.2.73	Model $H_{afwl}$ versus $S_w$ curves for L5 lithofacies .....	4-100
4.2.74	Model $H_{afwl}$ versus $S_w$ curves for L7 lithofacies .....	4-101
4.2.75	Model $H_{afwl}$ versus $S_w$ curves for L8 lithofacies .....	4-101
4.2.76	Model $H_{afwl}$ versus $S_w$ curves for L6 lithofacies .....	4-102
4.2.77	Model $H_{afwl}$ versus $S_w$ curves for L9 lithofacies .....	4-102
4.2.78	Model $H_{afwl}$ versus $S_w$ curves for all lithofacies at $\alpha = 10\%$ .....	4-103
4.2.79	Crossplot of brine and <i>in situ</i> Klinkenberg permeability .....	4-104
4.2.80	Relative gas permeability curves for 32 samples of different lithofacies.....	4-105
4.2.81	Single-saturation relative gas permeability data for sandstones .....	4-106
4.2.82	Drainage water relative permeability curves for 32 samples .....	4-107
4.2.83	Frequency distribution of $k_v/k_h$ ratio for continental lithofacies .....	4-108
4.2.84	Difference between Chase and Council Grove continental $k_v/k_h$ ratio.....	4-108
4.2.85	Frequency distribution of $k_v/k_h$ ratio for marine lithofacies .....	4-109
4.2.86	Difference between Chase and Council Grove marine $k_v/k_h$ ratio .....	4-109
4.2.87	Frequency distribution of $k_v/k_h$ ratio for limestone lithofacies .....	4-110
4.2.88	Difference between Chase and Council Grove limestone $k_v/k_h$ ratio.....	4-110
4.2.89	Frequency distribution of $k_v/k_h$ ratio for dolomite lithofacies .....	4-111
4.2.90	Difference between Chase and Council Grove dolomite $k_v/k_h$ ratio .....	4-111
4.2.91	Crossplot of full-diameter and plug porosity for Flower A-1 well.....	4-112
4.2.92	Crossplot of full-diameter and plug permeability for Flower A-1 well.....	4-113
4.2.93	Crossplot of full-diameter/plug permeability and porosity -Flower A-1 .....	4-114
4.2.94	Crossplot of plug- and DST-measured permeability for Flower A-1 well....	4-115
4.2.95	Crossplot of <i>in situ</i> Archie cementation exponent versus porosity.....	4-116
4.2.96	Frequency distribution of Archie cementation exponents .....	4-117
4.2.97	Frequency distribution of Archie saturation exponents .....	4-118
4.2.98	Crossplot of Archie saturation exponent versus porosity .....	4-119
4.3.1	Crossplot of wireline log density and core porosity by facies .....	4-124

4.3.2	Example of strong gas effect on neutron and density porosity logs .....	4-125
4.3.3	Crossplot of neutron-density porosity in Towanda limestone .....	4-126

**Chapter 5: Technology to Manage Large Digital Datasets**

5.1	Neural network employed for prediction of lithofacies .....	5-7
5.2	Worksheet for generating depositional environment and relative position ...	5-7
5.3	Output file containing depositional environment and relative position.....	5-8
5.4	Training variable selection dialog box in Kipling2.xla. ....	5-9
5.5	Neural network parameter dialog box in Kipling2.xla. ....	5-9
5.6	Objective function plot during neural network training process. ....	5-10
5.7	Dialog box matching log mnemonics to names, batch facies prediction.....	5-10
5.8	Output LAS file produced by the batch prediction process.....	5-11
5.9	Peak-and-shoulder removal process for washout correction .....	5-11
5.10	Input spreadsheet for porosity correction code.....	5-12
5.11	Bracketing search to find free water level elevation.....	5-13

**Chapter 6: Static Reservoir Model**

6.1	Workflow diagram for field-scale Hugoton model.....	6-27
6.2	Formation- and member-level stratigraphy correlated to wire-line well log.	6-28
6.3A	Map locating 1600 node wells used for the static model construction .....	6-29
6.3B	Map locating 8850 wells used for model structural framework .....	6-29
6.4	Single hidden-layer neural network used to predict lithofacies.....	6-30
6.5	Comparison of predicted lithofacies versus core-defined lithofacies .....	6-31
6.6	Distribution of Hugoton cores for which lithofacies were defined.....	6-32
6.7	Cross-validation analysis for optimal values neural network parameters ....	6-33
6.8	Empirical vertical variograms for lithofacies 5 .....	6-34
6.9	Empirical horizontal variograms for lithofacies 5 .....	6-34
6.10	Model lithofacies in stratigraphic cross-sections across the Hugoton shelf ..	6-35
6.11	Fence diagrams of Hugoton lithofacies model .....	6-37
6.12	Distribution of selected model lithofacies in 2-D map view .....	6-39
6.13	Map views of L7 lithofacies connected volumes in Council Grove.....	6-40
6.14	Map view of L6 and L10 lithofacies connected volumes in C_LM .....	6-41
6.15	Map view of pay lithofacies connected volumes in Chase .....	6-42
6.16	Map view of L0 lithofacies connected volumes in Council Grove .....	6-43
6.17	Map view of L10 lithofacies connected volumes in Chase .....	6-44
6.18	3-D view of connected volumes illustrating Krider ooid-bioclast shoal .....	6-45
6.19	3-D view of connected volumes illustrating B5_LM algal mounds .....	6-46
6.20	Property distribution in cellular Hugoton model in cross-section .....	6-47
6.21	Empirical vertical variograms for porosity in lithofacies 5 .....	6-48
6.22	Empirical horizontal variograms for porosity in lithofacies 5 .....	6-48
6.23	Upscaled lithofacies, porosity and permeability for Flower A-1 well.....	6-49
6.24	Crossplot, upscaled layer permeability vs. upscaled half-ft bed perm. ....	6-50
6.25	Frequency distribution of ratio of layer permeability to bed permeability ....	6.51
6.26	Crossplot of permeabilities, model zone vs. half-foot bed upscaled zone.....	6.52

**Chapter 7: Water Saturations and Free-Water Level**

7.1.1 Model  $H_{afwl}$  versus  $S_w$  curves for all lithofacies at  $\alpha = 10\%$  .....7-25  
7.1.2 Example model  $H_{afwl}$  versus  $S_w$  curves for continental L0 lithofacies .....7-25  
7.2.1 Two views of free-water level surface in Geomod4.....7-26  
7.2.2 Height above FWL for key stratigraphic horizons .....7-27  
7.2.3 Elevation above sea level for base of Chase and Council Grove .....7-28  
7.2.4 Average water saturation for Krider from wireline logs.....7-29  
7.2.5 Back-calculated FWL for eight wells in Texas County, Oklahoma .....7-29  
7.2.6 Geomod4-3 FWL from integration of three methods .....7-30  
7.3.1 Crossplot of  $H_{afwl}$ - $S_w$  curve parameter  $H_{te}$  and  $H_f$  errors .....7-31  
7.3.2 Crossplot of  $H_{afwl}$ - $S_w$  curve parameter  $H_{te}$  and  $H_f$  errors for continental .....7-32  
7.3.3 Crossplot of  $H_{afwl}$ - $S_w$  curve parameter  $H_{te}$  and  $H_f$  errors for marine .....7-33  
7.3.4 Crossplot of  $H_{afwl}$ - $S_w$  curve parameter  $H_{te}$  and  $H_f$  errors for limestones .....7-34  
7.3.5 Crossplot of  $H_{afwl}$ - $S_w$  curve parameter  $H_{te}$  and  $H_f$  errors for dolomites .....7-35  
7.3.6 Crossplot of  $H_{afwl}$ - $S_w$  curve parameter  $H_{te}$  and  $H_f$  errors for all .....7-36  
7.3.7 Example range in  $H_{afwl}$ - $S_w$  curve for packstone/grainstone with  $\alpha = 16\%$ ....7-37  
7.3.8 Frequency distribution of  $S_w$  difference between models 7-38

**Chapter 8: Reservoir Communication**

8.1.1 Crossplot of full-diameter and plug porosity for Flower A-1 well.....8-7  
8.1.2 Crossplot of full-diameter and plug permeability for Flower A-1 well.....8-8  
8.1.3 Crossplot of full-diameter/plug permeability and porosity -Flower A-1 .....8-9  
8.1.4 Crossplot of layered rock properties and porosity .....8-10  
8.1.5 Crossplot of routine permeability and porosity for all core.....8-11  
8.1.6 Crossplot of core- and DST-measured permeability for Flower A-1 well ...8-12  
8.1.7 Crossplot of core- and DST-measured permeability for several wells .....8-13  
8.1.8 Matrix-fracture permeability models for Hugoton .....8-14  
8.2.1 Basic end-member permeability averaging models.....8-19  
8.2.2 Reservoir simulation model .....8-20  
8.2.3 Cumulative gas recovery vs. time for models- variable thin-bed  $k$  .....8-21  
8.2.4 Cumulative gas recovery vs. time for thin-beds alone.....8-22  
8.2.5 Cumulative gas recovery vs. time for models – variable  $k_v$ .....8-23  
8.2.6 Dependence of incremental gas recovery on  $k_v$  .....8-24  
8.2.7 Example images showing change in pressure for variable  $k_v$  .....8-25  
8.2.8 Properties of siltstones and role as vertical flow barriers .....8-26  
8.3.1 Hugoton and Panoma field boundaries .....8-35  
8.3.2 Four scenarios for reservoir communication .....8-35  
8.3.3 Composite average Panoma and Hugoton initial WHSIP through time .....8-36  
8.3.4 Panoma and Hugoton composite WHSIP through time – Grant County.....8-36  
8.3.5 Composite WHSIP vs. cumulative gas for infill wells – Grant County .....8-37  
8.3.6 Composite P/Z vs. cumulative gas for nine Panoma wells – Grant County ..8-37  
8.3.7 Composite WHSIP vs. cumulative gas for wells in Fig. 8.3.6.....8-38  
8.3.8 Composite of long-term WHSIP – Stevens County .....8-38  
8.3.9 Relationship of Panoma isobar surface to Ft. Riley dip surface- Grant Co...8-39  
8.3.10 Hugoton and Panoma WHSIP and F. Riley dip surface- Grant Co. ....8-39  
8.3.11 Panoma 1983 isobar surface with Ft. Riley dip surface - Grant Co. ....8-40

8.3.12	First derivative of Ft. Riley structure for Hugoton and Flower well area.....	8-40
8.3.13	Panoma with Ft. Riley dip map at 1983- Grant Co.....	8-41
8.3.14	Core image of vertical fracture in Krider core.....	8-41
8.3.15	Regular space joints in Ft. Riley member quarry, SW Kansas.....	8-41
8.4.1	Simulator-calculated pressure distribution around Alexander D1&D2.....	8-44
8.4.2	Simulator-calculated pressures in Flower area – Jan 1970.....	8-45
8.4.3	Simulator-calculated pressures in Flower area – Jan 1995.....	8-46
8.4.4	Comparison between simulator- and DST-pressures by layer for Flower.....	8-47
8.4.5	Simulator-calculated pressures in Hoobler area – May 2006.....	8-48
8.4.6	Simulator-calculated pressures in select pay zones, Hoobler area .....	8-49
8.5.1	Study area in T. 31 S., R. 38 W., Stevens County, Kansas.....	8-69
8.5.2	Overburden gradient versus depth .....	8-69
8.5.3	Dipole sonic quality check for Chase Group, Flower A1 well.....	8-70
8.5.4	Dipole sonic quality check for Council Grove Group, Flower A1 well.....	8-70
8.5.5	Dipole sonic quality check for Chase Group, Youngren #1 well.....	8-71
8.5.6	Dipole sonic quality check for Council Grove Group, Youngren #1 well....	8-71
8.5.7	U matrix apparent from core-derived grain densities .....	8-72
8.5.8	Formation- and member-level stratigraphy correlated to wireline well log ..	8-73
8.5.9	Porosity vs. Young’s modulus with high correlation coefficient .....	8-74
8.5.10	Porosity vs. Young’s modulus rock-mechanical facies 1.....	8-74
8.5.11	Porosity vs. Young’s modulus rock-mechanical facies 2.....	8-75
8.5.12	Porosity vs. Young’s modulus rock-mechanical facies 3.....	8-75
8.5.13	Porosity vs. Young’s modulus rock-mechanical facies 4.....	8-76
8.5.14	Porosity vs. Young’s modulus rock-mechanical facies 5.....	8-76
8.5.15	Porosity vs. Young’s modulus rock-mechanical facies 6.....	8-77
8.5.16	Plot of model properties for upper Chase Group, Flower A1 well.....	8-78
8.5.17	Plot of model properties for middle Chase Group, Flower A1 well.....	8-79
8.5.18	Plot of model properties for lower Chase Group, Flower A1 well.....	8-80
8.5.19	Plot of model properties for upper Council Grove Group, Flower A1 well..	8-81
8.5.20	Plot of model properties for lower Council Grove Group, Flower A1 well..	8-82
8.5.21	Closure-analysis plot for microfrac test.....	8-83
8.5.22	Unit slope-wellbore storage plot.....	8-83
8.5.23	1960 Chase Group rock-mechanical properties.....	8-84
8.5.24	Fracture-simulation model fluid-viscosity profile .....	8-84
8.5.25	Simulated hydraulic-fracture dimensions, Chase parent well, 150 BPM.....	8-85
8.5.26	Simulated hydraulic-fracture permeability, Chase parent well, 150 BPM....	8-85
8.5.27	Simulated hydraulic-fracture conductivity, Chase parent well, 150 BPM....	8-86
8.5.28	Simulated hydraulic-fracture dimensions, Chase parent well, 300 BPM.....	8-86
8.5.29	Simulated hydraulic-fracture permeability, Chase parent well, 300 BPM....	8-87
8.5.30	Simulated hydraulic-fracture conductivity, Chase parent well, 300 BPM....	8-87
8.5.31	Static mechanical-properties plot, Chase parent well, 1960.....	8-88
8.5.32	Hydraulic-fracture dimensions, Chase parent well (1969), 300 BPM.....	8-88
8.5.33	Hydraulic-fracture permeability, Chase parent well (1969), 300 BPM.....	8-89
8.5.34	Hydraulic-fracture conductivity, Chase parent well (1969), 300 BPM.....	8-89
8.5.35	Hydraulic-fracture dimensions, Council Grove (1969), 162 BPM.....	8-90
8.5.36	Hydraulic-fracture permeability, Council Grove (1969), 162 BPM.....	8-90

8.5.37	Hydraulic-fracture conductivity, Council Grove (1969), 162 BPM	8-91
8.5.38	Static mechanical-properties plot, Chase infill well (1969)	8-91
8.5.39	Hydraulic-fracture dimensions, Chase infill (1987), 60 BPM	8-92
8.4.40	Hydraulic-fracture permeability, Chase infill (1987), 60 BPM	8-92
8.4.41	Hydraulic-fracture conductivity, Chase infill (1987), 60 BPM	8-93

**Chapter 9: Reservoir Simulation**

9.1.1	Location of simulation studies in Hugoton and Panoma fields	9-7
9.1.2	Pressures and GIP from Flower area simulation study	9-8
9.1.3	Pressures and GIP from Hoobler area simulation study	9-9
9.1.4	Pressures and GIP from Flower simulation study, 1946 and May 2004	9-10
9.1.5	GIP and produced volumes – Flower area	9-11
9.1.5	Gas and water relative-permeability curves for different rock-types	9-14
9.1.5	Range of possible gas relative-permeability values	9-15
9.2.1	Location of Alexander D1 & D2 and profile of D2	9-25
9.2.2	Bottom hole shut-in pressures at D1 and D2	9-26
9.2.3	Thin sections from two Council Grove lithofacies	9-27
9.2.4	Permeability-porosity recorded on plugs and whole cores	9-28
9.2.5	Development of permeability multiplier	9-29
9.2.6	Multipliers to convert plug permeability to whole-core permeability	9-30
9.2.7	Core photo showing microfractures – Youngren well, CG	9-31
9.2.8	Compare DST permeability with whole core permeability	9-32
9.2.9	Ratio of vertical to horizontal (maximum) permeability	9-33
9.2.10	Layer petrophysical parameters input to simulation studies	9-34
9.2.11	Conversion of surface shut-in pressure to bottom-hole shut-in condition	9-35
9.2.12	Location of D1 and D2 wells within the simulation study area	9-36
9.2.13	Summary of PVT properties used for simulation	9-37
9.2.14	RUN 1 results – Comparison of simulator-calculated production	9-38
9.2.15	RUN 1 results – Simulator-calculated pressure distribution	9-39
9.2.16	RUN 2 results - Comparison of simulator-calculated production	9-40
9.2.17	RUN 2 Results - Simulator-calculated bottom-hole flowing pressure	9-41
9.2.18	RUN 3 Results – Simulator-calculated flow rates	9-42
9.2.19	RUN 4 Results - Simulator-calculated flow rates	9-43
9.2.20	RUN 4 Results – Simulator-calculated pressures	9-44
9.2.21	RUN 5 Results – Simulator-calculated production	9-45
9.2.22	RUN 6 Results - Simulator-calculated flow rates	9-46
9.2.23	RUN 6 Results - Simulator-calculated bottom-hole flowing pressure	9-47
9.2.24	RUN 7 Results - Simulator-calculated flow rates	9-48
9.2.25	RUN 7 Results - Simulator-calculated bottom-hole flowing pressure	9-49
9.3.1	Map showing the location of the Flower study area	9-65
9.3.2	Map showing the location of wells in the Flower study area	9-66
9.3.3	Profile of study area type well Flower A-1 well	9-67
9.3.4	234-layer 3D volume of static model	9-68
9.3.5	Log data from wells used to model the larger Flower area P	9-69
9.3.6	Lithofacies-specific equations to estimate porosity from logs	9-70
9.3.7	Layer properties in fine- and up-scaled models	9-71

9.3.8	General PVT properties input to simulation study .....	9-72
9.3.9	Crossplot of <i>in situ</i> Klinkenberg permeability versus <i>in situ</i> porosity.....	9-73
9.3.10	Crossplot of full-diameter core porosity versus plug porosity.....	9-74
9.3.11	Comparison of DST permeability with full-diameter core permeability .....	9-75
9.3.12	Layer-specific permeability multiplier and upscaled layer permeability .....	9-76
9.3.13	Start dates of and initial shut-in (SI) pressures at Chase Parent wells.....	9-77
9.3.14	BHSP from well head shut-in pressure, WHSP = 422 psi.....	9-78
9.3.14B	BHSP from well head shut-in pressure, WHSP = 385 psi .....	9-79
9.3.15	RUN 1 - Simulator-calculated rate and pressure, Chase Parent wells .....	9-80
9.3.16	RUN 1 - Simulator-calculated rate and pressure, Chase Infill wells .....	9-81
9.3.17	RUN 1 - Simulator-calculated cum production, Council Grove wells .....	9-82
9.3.18	RUN 1 - Simulator-calculated reservoir pressure distribution, 1970 .....	9-83
9.3.19	RUN 2 - Simulator-calculated cum and pressure, Chase Parent wells .....	9-84
9.3.20	RUN 2 - Simulator-calculated rate and pressure, Chase Parent wells .....	9-85
9.3.21	RUN 2 - Simulator-calculated cum and pressure, Chase Infill wells .....	9-86
9.3.22A	RUN 2 - Simulator-calculated cum and pressure, Council Grove wells ....	9-87
9.3.22B	RUN 2 - Simulator-calculated cum and pressure, Council Grove wells.....	9-88
9.3.23	RUN 3 - Simulator-calculated rate, Chase Parent wells .....	9-89
9.3.24	RUN 3 - Simulator-calculated pressure, Chase Parent wells.....	9-90
9.3.25A	RUN 3 - Simulator-calculated rate, Council Grove wells .....	9-91
9.3.25B	RUN 3 - Simulator-calculated rate, Council Grove wells.....	9-92
9.3.26A	RUN 4 - Simulator-calculated rate, Council Grove wells .....	9-93
9.3.26B	RUN 4 - Simulator-calculated rate, Council Grove wells.....	9-94
9.3.27	RUN 5 - Simulator-calculated rate, Chase Parent wells .....	9-95
9.3.28A	RUN 5 - Simulator-calculated rate, Council Grove wells .....	9-96
9.3.28B	RUN 5 - Simulator-calculated rate, Council Grove wells.....	9-97
9.3.29	RUN 6 - Simulator-calculated rate, Chase Parent wells .....	9-98
9.3.30	RUN 6 - Simulator-calculated pressure, Chase Parent wells.....	9-99
9.3.31A	RUN 6 - Simulator-calculated rate, Council Grove wells .....	9-100
9.3.31B	RUN 6 - Simulator-calculated rate, Council Grove wells.....	9-101
9.3.32A	RUN 6 - Simulator-calculated pressure, Council Grove wells .....	9-102
9.3.32B	RUN 6 - Simulator-calculated pressure, Council Grove wells .....	9-103
9.3.33	RUN 6 - Simulator-calculated rate, Chase Infill wells .....	9-104
9.3.34	RUN 6 - Simulator-calculated pressure, Chase Parent wells.....	9-105
9.3.35	RUN 6 - Simulator-calculated reservoir pressure, 1970 .....	9-106
9.3.36	RUN 6 - Simulator-calculated shut-in pressure at Council Grove well.....	9-107
9.3.37	RUN 6 - Simulator-calculated pressure distribution, 1995.....	9-108
9.3.38	RUN 6 - Simulator-calculated layer pressure at Flower A1 .....	9-109
9.3.39	RUN 7 - Simulator-calculated shut-in pressure at Council Grove well.....	9-110
9.3.40	RUN 7 - Simulator-calculated layer pressure at Flower A1 .....	9-111
9.3.41	Simulator-calculated layer pressure at Flower A1, RUN 6 & 7.....	9-112
9.3.42	RUN 7 - Simulator-calculated layer pressure at Flower A1, 1995 & 2004...9-113	
9.3.43	RUN 7 - Simulator-calculated reservoir pressure distribution, 2004 .....	9-114
9.3.44	RUN 7 - Simulator-calculated annual production decline rates .....	9-115
9.3.45	RUN 8 - Simulator-calculated rate, Council Grove wells .....	9-116
9.3.46	Compare simulator-calculated layer pressure, RUN 7 & 8 .....	9-117

9.4.1	Map showing location of Graskell study area.....	9-128
9.4.2	Map showing the 12-square-mile Graskell study area.....	9-129
9.4.3	Map showing well locations inside Graskell study area.....	9-130
9.4.4	Fine-scale petrophysical models around Graskell study area.....	9-131
9.4.5	Structure on the free-water-level (FWL) surface, Graskell study area.....	9-132
9.4.6	Original-gas-in-place (OGIP) charging the Graskell model.....	9-133
9.4.7	PVT properties used in simulation studies on Graskell study area.....	9-134
9.4.8	Layer-specific permeability multipliers.....	9-135
9.4.9	Date of initial production and first recorded surface shut-in pressures.....	9-136
9.4.10	Layer-specific gas-in-place, initial pressure = 440 psi.....	9-137
9.4.11	Well information – Chase Parent and Council Grove.....	9-138
9.4.12	Well information – Chase Infill.....	9-139
9.4.13	RUN 1 - Simulator-calculated cumulative gas, Chase Parent wells.....	9-140
9.4.14	RUN 1 - Simulator-calculated cumulative gas, Chase Parent wells.....	9-141
9.4.15	RUN 1 - Simulator-calculated cumulative gas, Council Grove wells.....	9-142
9.4.16	RUN 1 - Simulator-calculated cumulative gas, Council Grove wells.....	9-143
9.4.17	RUN 2 - Simulator-calculated cumulative gas, Chase Parent wells.....	9-144
9.4.18	RUN 2 - Simulator-calculated cumulative gas, Chase Parent wells.....	9-145
9.4.19	RUN 3 - Simulator-calculated cumulative gas, Chase Parent wells.....	9-146
9.4.20	RUN 3 - Simulator-calculated cumulative gas, Chase Parent wells.....	9-147
9.4.21	RUN 4 - Simulator-calculated cumulative gas, Chase Parent wells.....	9-148
9.4.22	RUN 4 - Simulator-calculated cumulative gas, Chase Parent wells.....	9-149
9.4.23	Original-gas-in-place and permeability distribution in Layer 8.....	9-150
9.4.24	RUN 5 - Simulator-calculated cumulative gas, Chase Parent wells.....	9-151
9.4.25	RUN 5 - Simulator-calculated cumulative gas, Chase Parent wells.....	9-152
9.4.26	Cross section and map showing location of wells with RFT data.....	9-153
9.4.27	Simulator-calculated layer pressure, Dec 2004, at Eliot A6 vs. RFT.....	9-154
9.4.28	RUN 6 & 7 - Simulator-calculated cumulative gas, Council Grove wells....	9-155
9.4.29	RUN 6 & 7 - Simulator-calculated cumulative gas, Council Grove wells....	9-156
9.4.30	RUN 8 - Simulator-calculated cumulative gas, Council Grove wells.....	9-157
9.4.31	RUN 8 - Simulator-calculated cumulative gas, Council Grove wells.....	9-158
9.4.32	RUN 9 - Simulator-calculated pressure distribution, January 1978.....	9-159
9.4.33	RUN 9 - Simulator-calculated shut-in pressure, Council Grove well.....	9-160
9.4.34	First recorded shut-in pressures at Council Grove wells.....	9-161
9.4.35	RUN 10 - History matches at the Chase Parent wells.....	9-162
9.4.36	RUN 10 - History matches at the Chase Parent wells.....	9-163
9.4.37	RUN 10 - History matches at the Council Grove wells.....	9-164
9.4.38	RUN 10 - History matches at the Council Grove wells.....	9-165
9.4.39	RUN 10 - History matches at the Chase Infill wells.....	9-166
9.4.40	RUN 10 - History matches at the Chase Infill wells.....	9-167
9.4.41	RUN 10 - Rate and pressure history matches at the Chase Infill wells.....	9-168
9.4.42	RUN 10 - Rate and pressure history matches at the Chase Infill wells.....	9-169
9.4.43	Location of Chase Infill wells where history match failed.....	9-170
9.4.44	Simulator-calculated shut-in pressure at a Council Grove well, 1978.....	9-171
9.4.45	RUN 10 - Simulator-calculated layer pressures at Eliot A well.....	9-172
9.4.46	RUN 11 - Simulator-calculated shut-in pressure at Council Grove well.....	9-173

9.3.47	Simulator-calculated layer pressures at Eliot A6, 2004, Run 10 and 11 .....	9-174
9.5.1	Map showing location of the Hoobler study area .....	9-186
9.5.2	Map showing the locations of the Chase wells in the Hoobler area .....	9-187
9.5.3	Map showing node wells in and around the Hoobler study area .....	9-188
9.5.4	Map showing location of wells with available RFT data .....	9-189
9.5.5	Map view of water saturation for top layer in the Herington .....	9-190
9.5.6	Porosity, permeability, and water saturation upscaled to 24 layers .....	9-191
9.5.7	Distribution GIP in 11-layer model, FWL +65 ft above sea level.....	9-192
9.5.8	Distribution of upscaled petrophysical properties in the Hoobler model .....	9-193
9.5.9	Lithofacies-specific equations to estimate porosity from logs .....	9-194
9.5.10	PVT properties input to the simulator.....	9-195
9.5.11	Whole-core porosity and permeability measurements, Chase intervals .....	9-196
9.5.12	Layer-specific permeability multipliers.....	9-197
9.5.13	Plot of surface shut-in pressures at Chase wells .....	9-198
9.5.14	Conversion of surface shut-in pressures to sub surface shut-in pressures .....	9-199
9.5.15	Layer-specific gas-in-place (GIP) in the geomodel .....	9-200
9.5.16	Start date, completion intervals, cumulative production of Chase wells.....	9-201
9.5.17	Initial-completion records of Chase wells .....	9-202
9.5.18	RUN 1 - Simulator-calculated cumulative production, Chase wells .....	9-203
9.5.19	RUN 1 - Production- and pressure-history matches, Chase wells .....	9-204
9.5.20	RUN 1 - Production- and pressure-history matches, Chase wells .....	9-205
9.5.21	Permeability distribution in Winfield (Layer 4) .....	9-206
9.5.22	Best-estimated layer pressures from RFT, 2005.....	9-207
9.5.23	RUN 1 - Calculated pressure, EW section through Hoobler EU well .....	9-208
9.5.24	RUN 2 - Simulator-calculated field production.....	9-209
9.5.25	RUN 2 - Calculated pressure, EW section through Hoobler EU well .....	9-210
9.5.26	RUN 3 - Simulator-calculated field production.....	9-211
9.5.27	RUN 3 - Calculated pressure, EW section through Hoobler EU well .....	9-212
9.5.28	RUN 4 - Simulator-calculated field production.....	9-213
9.5.29	RUN 4 - Gas-in-place in Herington through time .....	9-214
9.5.30	RUN 4 - Calculated pressure, EW section through Hoobler EU well .....	9-215
9.5.31	Whole-core porosity and permeability from Herington zone .....	9-216
9.5.32	RUN 5 - Simulator-calculated field production.....	9-217
9.5.33	RUN 6 - Simulator-calculated field production.....	9-218
9.5.34	RUN 7 - Simulator-calculated field production.....	9-219
9.5.35	RUN 7 – Production and pressure history matches at Chase wells .....	9-220
9.5.36	RUN 7 – Production and pressure history matches at Chase wells .....	9-221
9.5.37	RUN 7 - Calculated pressure, EW section through Hoobler EU well .....	9-222
9.5.38	RUN 7 – Simulator-calculated GIP in top 6 Chase layers.....	9-223
9.5.39	RUN 8 – Production and pressure history matches at Chase wells .....	9-224
9.5.40	RUN 8 – Production and pressure history matches at Chase wells .....	9-225
9.5.41	RUN 9 - Production and pressure history match, at Blk28P well .....	9-226
9.5.42	RUN 9 – GIP in Fort Riley through time and layer permeabilities .....	9-227
9.5.43	RUN 10 – Production and pressure history matches at Chase wells .....	9-228
9.5.44	RUN 10 – Production and pressure history matches at Chase wells .....	9-229
9.5.45	RUN 11 – Production and pressure history matches at Chase wells .....	9-230

9.5.46	RUN 11 – Production and pressure history matches at Chase wells .....	9-231
9.5.47	RUN 11 - Qualitative estimate of history matches at each well .....	9-232
9.5.48	RUN 11 – Simulator-calculated layer pressure vs. RFT pressure .....	9-233
9.5.49	RUN 11 – GIP in Fort Riley through time.....	9-234
9.6.1	Expected profiles of P/z vs. Gp curves for different drive mechanisms.....	9-243
9.6.2	Map showing location of Alexander D1 and D2 wells.....	9-244
9.6.3	Plot of P/z vs. Gp data from Alexander D1 until 1975 .....	9-245
9.6.4	Plot of P/z vs. Gp data from Alexander D1 until 1990.....	9-246
9.6.5	Bottom-hole shut-in pressures recorded at Alexander D1 and D2 wells.....	9-247
9.6.6	Map showing location of Flower study area.....	9-248
9.6.7A	P/z vs. Gp plots for Chase Parent wells in the Flower study area .....	9-249
9.6.7E	P/z vs. Gp plots for Chase Parent wells in the Flower study area .....	9-250
9.6.7I	P/z vs. Gp plots for a Chase Parent well in the Flower study area .....	9-251
9.6.8	Start dates of Council Grove and Chase Infill wells, Flower area.....	9-252
9.6.9	Map showing location of Hoobler study area.....	9-253
9.6.10A	P/z vs. Gp plots for Hoobler area Chase wells, completions to L4.....	9-254
9.6.10E	P/z vs. Gp plots for Hoobler area Chase wells, completions to L4.....	9-255
9.6.11	P/z vs. Gp plots for Hoobler area Chase wells, uncertain initial histories.....	9-256
9.6.12	P/z vs. Gp plots for Hoobler area Chase wells, completions to L6 .....	9-257
9.6.13	Location of Muller and Williams wells and their history matches.....	9-258
9.6.14	P/z vs. Gp plots for Muller and Williams .....	9-259

***Chapter 10: Original and Remaining Gas in Place***

10.1.1	Simulations of record in the Hugoton and Panoma fields .....	10-11
10.1.2	Hugoton field cumulative production vs. volumetric OGIP.....	10-12
10.1.3	Grant and Stevens cumulative production vs. volumetric OGIP .....	10-13
10.1.4	Wolfcamp recovery efficiency (cumulative production/OGIP) .....	10-14
10.1.5	Hugoton county index and core wells.....	10-15
10.2.1	Location of 38 wells having pressures by zone .....	10-24
10.2.2	Combined production for 28 Flower model wells projected through 2050...10-25	
10.2.3	Chase zone pressures through time by zone plot.....	10-26
10.2.4	Council Grove pressures through time by zone plot.....	10-27
10.2.5	Fort Riley connected volumes with low permeability and water saturation..10-28	

***Appendices***

Appendices provide supplemental information and data in an informal format.

- Geomod4\_variograms.pdf
- Geomod4\_build.pdf
- CORE\_DATA&DESCRIPTIONS\_DATABASE.xls
- BatchCurveProcessing.pdf
- BatchCurveProcessing.xls

# CHAPTER 1. INTRODUCTION

*Martin K. Dubois and Alan P. Byrnes*

The Hugoton and Panoma fields represent a major resource for the companies that own leases, royalty owners, and the state of Kansas. Although these fields have been producing for over 70 years there is much that is not fully understood about the nature of original and remaining gas-in-place, distribution of lithofacies, and the properties of the rocks that control reserves and production. To be able to efficiently manage the field at the lease- to field-scale an accurate static and dynamic model(s) of the fields was needed. This report is a result of a collaborative, multi-disciplinary study (Hugoton Asset Management Project (HAMP)) conducted by the Kansas Geological Survey and industry partners from 2004 through 2006. It follows a five-year study, the “Hugoton Project” (1998-2003) where the primary focus was on building a comprehensive geologic tops database. In the last few years of the Hugoton Project a cellular geomodel for the Council Grove (Panoma) in Kansas (Geomod1) was built in collaboration with Pioneer, where Shane Seals provided Petrel™ modeling with the assistance of David Hamilton, SCM, Inc. Industry partners as well as KGS staff were encouraged by the results and the methods, and the workflow developed served as an initial template for the more ambitious HAMP models of the entire Permian gas system in Kansas and Oklahoma. The nine-industry partner HAMP, later expanded to ten (five from Hugoton plus five new participants), was begun in January 2004 as a two-year project. Building an accurate static model for the entire Hugoton field (Hugoton and Panoma in Kansas and Guymon-Hugoton in Oklahoma) became the primary objective in the Hugoton Asset Management Project (HAMP) with the goal of developing a model with sufficient detail to represent vertical and lateral heterogeneity at the well, multi-well, and field scale, that could be used as a tool for reservoir management.

Importance of the Hugoton field study extends beyond the borders of Kansas and Oklahoma. Both the knowledge gained and the techniques employed have implications for understanding and modeling reservoir systems worldwide that have similar geologic age, reservoir architecture, production characteristics, problems in determining water saturation, large data sets, multiple operators, or state of maturity. The full-field model of the 10,000-mi<sup>2</sup> (26,000-km<sup>2</sup>) reservoir area provides a detailed three-dimensional view of thirteen shoaling-upward cycles vertically stacked in a low-relief shelf setting. The nature of the model and its construction provide a good analog for similar thin, stacked-cycle reservoir systems including the Aneth field in the Paradox basin (Weber et al., 1994; Grammer et al., 1996), fields in the prolific Permian basin of west Texas (Dutton et al., 2005), and the Khuff Formation in Gwahar and North fields in the Arabian Gulf (McGillivray and Hussein, 1992; Konnert et al., 2001). Fine-scale cellular models are particularly important for modeling thin-layered, differentially depleted reservoir systems, and methods used in building the model demonstrate the construction of a cellular petrophysical model for a giant field. The project also demonstrates the benefits of pooling proprietary geologic and engineering data in settings having multiple operators (Sorenson, 2005). As the world’s giant fields mature, high-resolution modeling at the full-field scale in data-rich environments will become increasingly important.

## Approach

Building an accurate static model for the entire Hugoton field (Hugoton and Panoma in Kansas and Guymon-Hugoton in Oklahoma) was the primary objective in the Hugoton Asset Management Project (HAMP). The goal was to develop a model with sufficient detail to represent vertical and lateral heterogeneity at the well, multi-well, and field scale, which could be used as a tool for reservoir management including accurate prediction of remaining-gas-in-place. This required that the model be finely layered (169 layers, 3-foot (1 m) average thickness), and have relatively small XY cell dimensions (660x660 ft, 200x200m; 64 cells per mi<sup>2</sup>). These criteria resulted in development of a 108-million cell model for the 10,000-mi<sup>2</sup> (26,000 km<sup>2</sup>) area modeled. Although lithofacies geobodies tend to be laterally extensive, covering multi-section to township scales, small XY cell dimensions were required to allow the extraction of portions of the model for local reservoir simulation. Water saturations needed for original gas-in-place (OGIP) determination were estimated using capillary pressure methods and not measurements from induction wireline logs because accurate determination of water saturations using conventional wireline logs is complicated by deep mud filtrate invasion for typical drilling programs (Olson et al., 1997; George et al., 2004). Material balance methods for estimating OGIP are equally problematic because the reservoir is layered and differentially depleted and wellhead shut-in pressures (WHSIP) are strongly influenced by high-permeability interval properties, and do not accurately represent all interval pressures; and pressure data for individual layers are sparse. The Hugoton geomodel may be the largest model of its kind (lithofacies-controlled, property-based water saturations).

The general workflow for developing the Hugoton geomodel shown in Figure 1.1 can be characterized as comprising four principal steps: 1) Compile data for stratigraphy (formation tops) and core lithologic properties, petrophysical properties, wireline logs, fluid properties, and production and analyze data to certify that the data meet quality and accuracy criteria; 2) Define properties/develop algorithms including training a neural network and predicting lithofacies at node wells and developing wireline-log analysis algorithms (including corrections) and petrophysical properties algorithms (e.g., permeability-porosity ( $k-\phi$ ), capillary pressure ( $P_c$ ), relative permeability( $k_r$ )), 3) Develop databases of properties for use in geomodel construction including lithofacies, porosity, tops, free-water level at node wells, and 4) Develop geomodel by constructing 3-D cellular model using tops database, populating node-well cells with lithofacies and porosity database properties, upscaling properties as appropriate and populating 3-D model with basic properties, then utilizing petrophysical algorithms, populate 3-D cellular model with lithofacies-specific petrophysical properties and fluid saturations. Not illustrated in the static model workflow diagram, are reservoir simulations performed on upscaled portions of intermediate and final static models in different geologic settings. Simulations were performed concurrent with model building and served to validate the static model properties and model workflow. Chapters of this report summarize key aspects of the workflow as discussed below.

## Background and Prior Work

The combined Kansas Hugoton and Panoma, Texas Hugoton and West Panhandle fields, and Oklahoma Guymon-Hugoton, with an estimated ultimate recovery of 75 tcf (2.1 trillion m<sup>3</sup>) gas (Sorenson, 2005) represent the largest gas field in North America. Covering southwest Kansas and portions of the Oklahoma and Texas panhandles; these fields are situated in the Hugoton embayment of the Anadarko basin (Figure 1.2). Since discovery in 1922 and development in the 1950's, 35 trillion standard cubic ft gas (tcf, 963 billion m<sup>3</sup>) have been produced from >12,000 wells over 6200 mi<sup>2</sup> (16,000 km<sup>2</sup>) in the Kansas and Oklahoma portion of the Hugoton field (Figure 1.3). Unless otherwise noted, the term "Hugoton" in this report combines the Hugoton (Kansas), Panoma (Kansas and Oklahoma) and Guymon-Hugoton (Oklahoma) fields. Production is from the lower Permian Chase and Council Grove Groups (Figure 1.4) containing 13 stratigraphic intervals each comprising a wide range of lithofacies including continental and marine siltstones to sandstones, mudstone to grainstone limestones, fine- to medium-crystalline dolomites, and phylloid algal bafflestones (Figure 1.5). In most areas inside the Panoma field boundary, the gas column is continuous between the two stratigraphic intervals (Pippin, 1970; Parham and Campbell, 1993) and reaches a maximum thickness of 500 ft (150 m) in the west-central part of the study area. One exception may be in a relatively small portion of the field near the west margin in Morton County, Kansas, which is described by Olson et al. (1997) as being compartmentalized by faults. In Oklahoma, production outlined as "other Council Grove" (Figure 1.2) is from intervals in the Council Grove that are up to 300 ft (100 m) below the lowest perforations in the Chase. The reservoir is shallow, with depth to the top of the Chase ranging from 2100 to 2800 ft (640-850 m) and lower and upper productive limits, referenced to sea level, of approximately +100 ft (+30 m) on the east and +1250 ft (+380 m) on the western updip margin, respectively. Original wellhead shut-in pressure in Kansas was 437 psi (3013 kPa) (Hemsell, 1939), significantly less than half of a seawater pressure gradient, and similar, anomalously low initial pressures were recorded in Oklahoma (Sorenson, 2005). Average 72-hour wellhead shut-in pressure in Kansas in 2003 was 32 psi (221 kPa). Annual production in 2004 was 265 billion cubic ft (BCF, 7.5 billion m<sup>3</sup>). Early completions in the Chase were commonly open hole or used a slotted liner followed by a large acid treatment. After 1960 typical completions commonly involve casing, perforating and acidizing as many as six zones separately, followed by a large hydraulic-sand-fracture treatment, sometimes exceeding 200,000 lb (91,000 kg) of sand, to the entire perforated interval (Hecker et al., 1995).

Although much has been published on the Hugoton over the 70-year life of the field, most of the studies have been broad in scope (Hemsell, 1939; Mason, 1968; Pippin, 1970). Sorenson's (2005) recent paper presents a paleostructural and pressure history for the reservoir system stretching from the Texas Panhandle to west-central Kansas and provides a good recent overview of the field history and prior work. Detailed studies involving reservoir characterization have been limited geographically and stratigraphically. For example, Siemers and Ahr (1990) investigated the Chase in the Oklahoma panhandle, Olson et al. (1997) studied the Kansas Chase, and Heyer (1999) focused on the Council Grove in a small area of the Oklahoma Panhandle. Following the

Kansas Corporation Commission proration order permitting a second well in each unit, several studies on reservoir characterization (Seimers and Ahr; 1990; Caldwell, 1991; Olson et al., 1997) and reservoir simulation (Fetkovitch et al., 1994; Oberst et al., 1994) were published. The work by Fetkovitch et al. (1994) and Oberst et al. (1994) represent the only two reservoir simulations published to date, and neither included the Council Grove in their simulations. Past studies by industry have been generally confined to areas where they have assets and data. This report provides details of the most comprehensive reservoir characterization and simulation effort to date, both geographically (entire field) and stratigraphically (the entire reservoir system, Chase and Council Grove Groups).

## **Report Organization**

Figure 1.1 illustrates the general workflow process involved in construction of the Hugoton geomodel. This report is generally organized to cover key aspects of tasks and products involved in the workflow. We have attempted to write each chapter in a manner that it can stand alone, but in some cases the reader will be referred to other chapters or the subject is best understood in context of other chapters or the entire body of the report.

### **Chapter 1. Introduction**

A general overview of the project and this report, including some historical context, purpose of the study, problems, and approach is provided. Also covered is the importance of the field-wide geomodel as an example for similar layered reservoir systems worldwide. Earlier work by numerous authors is given a brief, but comprehensive review.

### **Chapter 2. Geologic Setting**

This chapter discusses the regional geologic and tectonic history of the Hugoton Embayment of the Anadarko basin with emphasis on the large-scale geometry and sedimentation pattern on the low-relief Hugoton shelf. A general description by prior authors of the “giant stratigraphic trap” is also provided.

### **Chapter 3. Depositional Model**

More detailed context for deposition of the 13 marine-continental, carbonate-siliciclastic cycles that compose the Hugoton reservoir system is developed, including evidence supporting a 1 ft/mi slope and a maximum of 100 ft of relief on the shelf. The influence of climate, shelf geometry, glacially forced sea level oscillation and their changes through Wolfcampian (icehouse towards greenhouse conditions) on lithofacies stacking patterns, lithofacies distribution patterns, and depositional models is presented.

### **Chapter 4. Reservoir Characterization**

This chapter covers the models/equations used in geomodel development including the digital lithofacies classification system, petrophysical properties equations (e.g., routine and *in situ* properties, lithofacies-specific permeability-porosity relations, capillary pressure relations, and relative permeability relations), and wireline porosity-log analysis.

## **Chapter 5. Technology to Manage Large Digital Datasets**

This chapter describes data management and the automated analysis tools developed to handle the large databases used for lithofacies-prediction and computation of porosities corrected for mineralogical variations between lithofacies and for washouts. Tools facilitated the efficient handling of large data volumes, and the ability to perform the multiple iterations required to test preliminary and intermediate algorithms and solutions.

## **Chapter 6. Static Reservoir Model**

Building an accurate static model for the entire Hugoton field was the primary objective in the study. This chapter discusses the overall workflow, and provides details on the construction of the lithofacies, porosity, and petrophysical models not covered in other chapters (e.g., lithofacies prediction using neural networks, lithofacies and porosity variogram analysis, and permeability upscaling). The resulting lithofacies model is examined in detail.

## **Chapter 7. Water Saturations and Free Water Level**

Due to frequent deep filtrate invasion during drilling water saturations estimated from wireline logs are problematic. Aspects of water saturation determination including the capillary-pressure properties of Hugoton rocks, the relationship between saturation and free water level, the FWL surface geometry, and sensitivity of the estimated water saturations and original-gas-in-place (OGIP) to capillary-pressure and FWL uncertainty are discussed.

## **Chapter 8. Reservoir Communication**

This chapter analyzes the relative contribution of lithofacies/beds within defined productive intervals and the nature of communication between intervals. It further examines the potential and evidence for communication between intervals (formation/member) and groups (Chase/Council Grove) by natural causes and hydraulic fracture stimulations.

## **Chapter 9. Reservoir Simulation**

Successfully matching pressure and production history at the well scale was an effective and important method for testing the validity of the static model(s) constructed. This chapter reviews the four simulation studies conducted, one single-well and three multi-well simulations, covering areas as large as 12-mi<sup>2</sup> and including up to 38 wells. Model inputs, pressure and production histories, model properties, and adjustments required of the model to acquire a match are documented through the entire simulation process in each case study.

## **Chapter 10. Original and Remaining Gas in Place**

A volumetric model of original-gas-in-place (OGIP) at the well- to field- scale is an outcome of the Hugoton cellular geomodel and one of the main products sought by HAMP. Model OGIP is compared with cumulative gas produced at varying scales and validates the static model and free-water-level elevation for most areas. Pore volumes (PV), hydrocarbon-pore volume (HCPV), and ratio of HCPV/PV by lithofacies illustrate

the relative contribution by the 11 lithofacies. Remaining GIP by zone is examined through analysis of simulation results and is discussed qualitatively with respect to the field static model.

### **Chapter 11. Conclusions**

In the final chapter we provide a comprehensive review that includes key findings, a detailed summary of the processes involved in building the model, discuss specific findings at the workflow component level, and suggest additional work that could improve the model and topics deserving further investigation.

### **References**

Baars, D. L., (compl.), 1994, Revision of stratigraphic nomenclature in Kansas, Kansas Geological Survey, Bulletin 230, 80 p.

Caldwell, C. D., 1991, Cyclic deposition of the Lower Permian, Wolfcampian, Chase Group, western Guymon-Hugoton field, Texas County, Oklahoma, *in* W. L. Watney, A. W. Walton, C. G. Caldwell, and M. K. Dubois, organizers: Integrated Studies of Petroleum Reservoirs in the Midcontinent: American Association of Petroleum Geologists, Midcontinent Section Meeting, Wichita, Kansas, p. 57-75.

Dubois, M.K., A.P. Byrnes, T.R. Carr, G.C. Bohling, and J.H. Doveton, *in press*, Multiscale geologic and petrophysical modeling of the giant Hugoton gas field (Permian), Kansas and Oklahoma, *in* P. M. Harris and L. J. Weber, eds., Giant reservoirs of the world: From rocks to reservoir characterization and modeling: American Association of Petroleum Geologists, Memoir 88.

Dutton, S. P., E. K. Kim, C. L. Broadhead, W. D. Raatz, S. C. Ruppel, and C. Kerans, 2005, Play analysis and digital portfolio of major oil reservoirs in the Permian Basin: Bureau of Economic Geology, Reports of Investigations, RI0271, 302 p.

Fetkovitch, M. J., D. JJ. Ebbs Jr., and J. J. Voelker, 1994, Multiwell, multilayer model to evaluate infill-drilling potential in the Oklahoma Hugoton field: Society of Petroleum Engineers, 65th Annual Technical Conference and Exhibition, New Orleans, Paper SPE 20778, p. 162-168.

George, B. K., C. Torres-Verdin, M. Delshad, R. Sigal, F. Zouioueche, and B. Anderson, 2004, Assessment of in-situ hydrocarbon saturation in the presence of deep invasion and highly saline connate water: *Petrophysics*, v. 45, no. 2, p. 141-156.

Grammer, G. M., G. P. Eberli, F. S. P. van Buchem, G. M. Stevenson, and P. Homewood, 1996, Application of high-resolution sequence stratigraphy to evaluate lateral variability in outcrop and subsurface, Desert Creek and Ismay intervals, Paradox Basin: *in* M. W.

Hecker, M. T., M. E. Houston, and J. D. Dumas, 1995, Improved completion designs in the Hugoton field utilizing multiple gamma emitting tracers: Society of Petroleum Engineers, Annual Technical Conference and Exhibition, Dallas, TX, Paper SPE 30651, p. 223-235.

Hemsell, C. C., 1939, Geology of Hugoton Gas Field of southwestern Kansas: American Association of Petroleum Geologists Bulletin, v. 23, no. 7, p. 1054-1067.

Heyer, J. F., 1999, Reservoir characterization of the Council Grove Group, Texas County, Oklahoma, *in* D. F. Merriam, ed., Geosciences for the 21<sup>st</sup> Century: Transactions of the American Association of Petroleum Geologists Midcontinent Section Meeting, Wichita, KS, p. 71-82.

Konnert, G., A. M. Afifi, S. A. Al-Hajri, K. de Groot, A. A. Al Naim, and H. J. Droste, 2001, Paleozoic stratigraphy and hydrocarbon habitat of the Arabian plate, *in* M. W. Downey, J. C. Threet, and W. A. Morgan, eds., Petroleum provinces of the twenty-first century: American Association of Petroleum Geologists Memoir 74, p. 483-515.

Mason, J. W., 1968, Hugoton and Panhandle field, Kansas, Oklahoma and Texas, *in* W. B. Beebe and B. F. Curtis, eds., Natural Gases of North America, v. 2, American Association of Petroleum Geologists Memoir 9, p. 1539-1547.

McGillivray, J. G., and M. I. Husseini, 1992, The Paleozoic petroleum geology of central Arabia: American Association of Petroleum Geologists Bulletin, v. 76, p. 1491-1506.

Oberst, R. J., P. P. Bansal and M. F. Cohen, 1994, 3-D reservoir simulation results of a 25-square mile study area in Kansas Hugoton gas field: Society of Petroleum Engineers Mid-Continent Gas Symposium, Amarillo, TX, Paper SPE 27931, p. 137-147.

Olson, T. M., Babcock, J. A., Prasad, K. V. K., Boughton, S. D., Wagner, P. D., Franklin, M. K., and Thompson, K. A., 1997, Reservoir characterization of the giant Hugoton Gas Field, Kansas: American Association of Petroleum Geologists, Bulletin, v. 81, p. 1785-1803.

Parham, K. D., and J. A. Campbell, 1993, PM-8. Wolfcampian shallow shelf carbonate-Hugoton Embayment, Kansas and Oklahoma: *in* D. G. Bebout, ed., Atlas of Major Midcontinent Gas Reservoirs: Gas Research Institute, p. 9-12.

Pippin, L., 1970, Panhandle-Hugoton field, Texas-Oklahoma-Kansas-The first fifty years, *in* Halbouty, M. T. (ed.), Geology of Giant Petroleum Fields: American Association of Petroleum Geologists, Memoir 14, Tulsa, p. 204-222.

Sawin, R. S., R. R. West, E. K. Franseen, W. L. Watney, and J. R. McCauley, 2006, Carbiniferous-Permian boundary in Kansas, mid-continent U.S.A, *in* Current Research in Earth Sciences: Kansas Geological Survey, Bulletin 252, part 2, <http://www.kgs.ku.edu/Current/2006/sawin/> (accessed August 23, 2006).

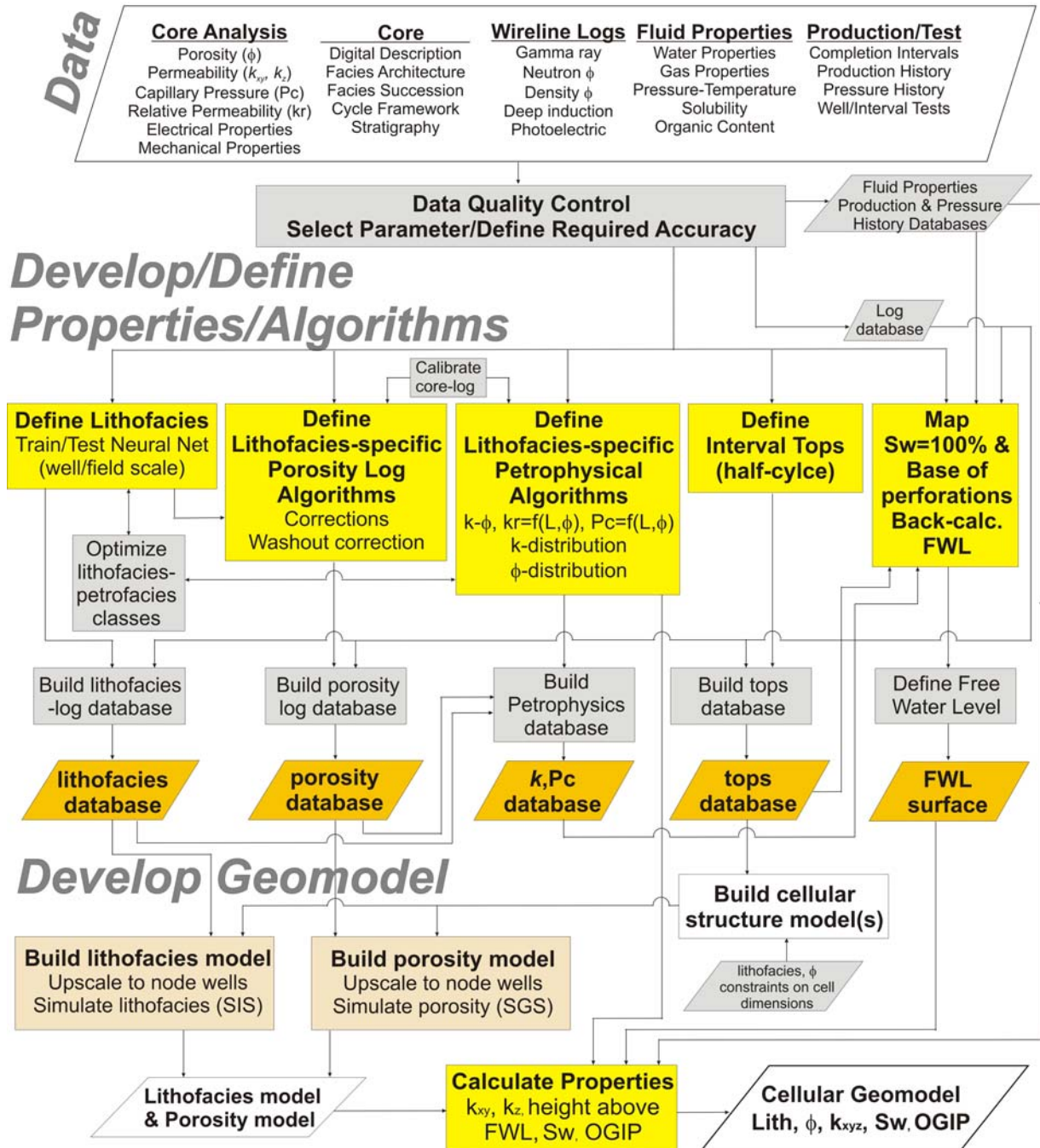
Siemers, W. T., and W. M. Ahr, 1990, Reservoir facies, pore characteristics, and flow units: Lower Permian Chase Group, Guymon-Hugoton Field, Oklahoma: Society of Petroleum Engineers Proceedings, 65th Annual Technical Conference and Exhibition, New Orleans, LA, September 23-26, 1990, Paper SPE 20757, p. 417-428.

Sorenson, R. P., 2005, A dynamic model for the Permian Panhandle and Hugoton fields, western Anadarko basin: American Association of Petroleum Geologists Bulletin, v. 89, no. 7, p. 921-938.

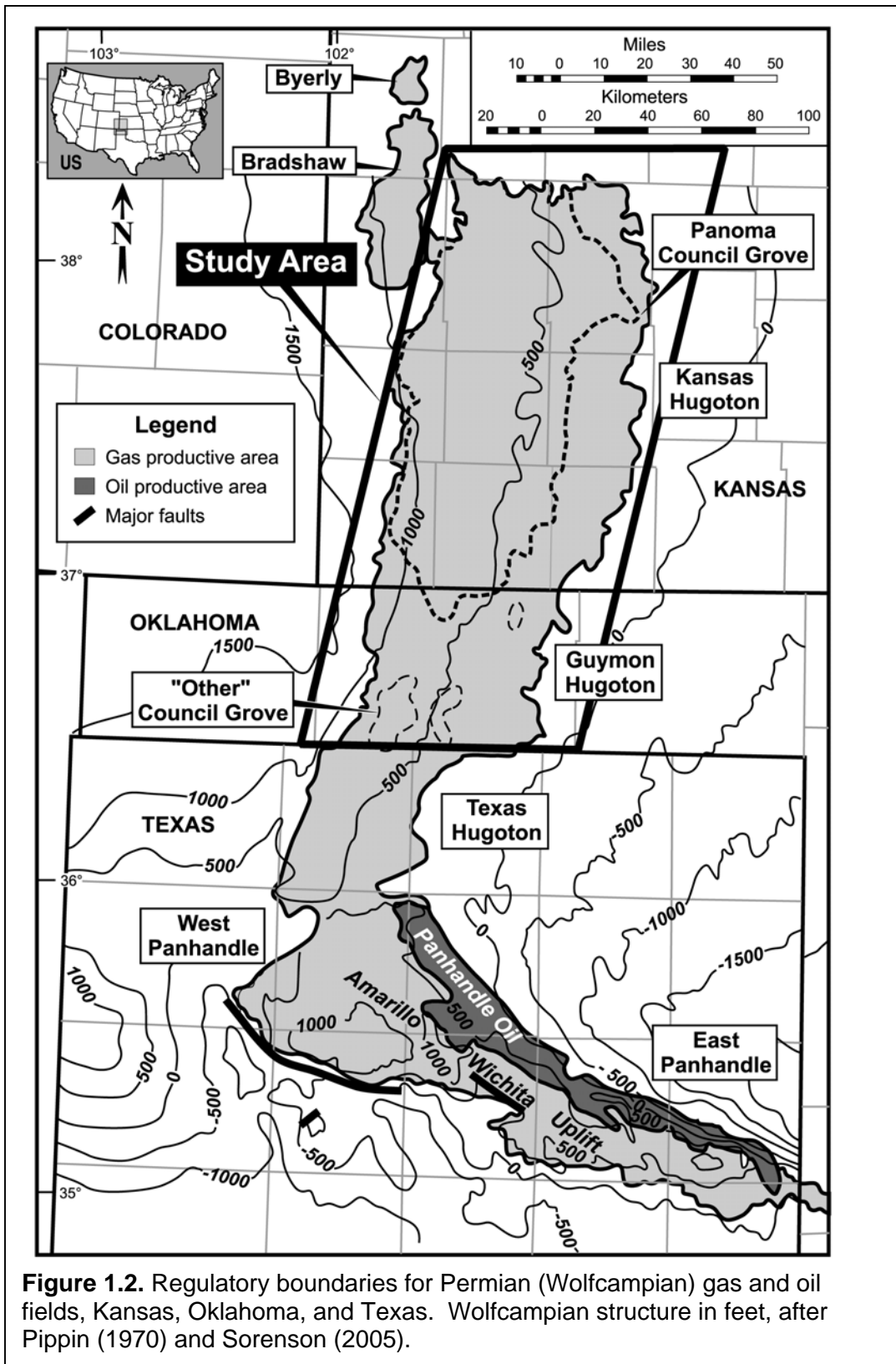
Weber, L. J., F. M. Wright, J. F. Sarg, E. Shaw, L. P. Harman, J. B., Vanderhill, and D. A. Best, 1994, Reservoir delineation and performance; application of sequence stratigraphy and integration of petrophysics and engineering data, Aneth field, southeast Utah, U.S.A.: *in* E. L. Stout and P. M. Harris, eds., Hydrocarbon Reservoir Characterization; Geologic Framework and Flow Unit Modeling: Society of Sedimentary Geology, Tulsa, OK, p. 1-29.

Zeller, D. E., ed., 1968, The stratigraphic succession in Kansas: Kansas Geological Survey, Bulletin 189, 81 p.

# Model Development Workflow



**Figure 1.1.** Workflow for field-scale Hugoton model. Workflow can be divided into three broad tasks: 1) gather and qualify data; 2) process data to provide basic geomodel input files (Develop/ Define/ Properties/ Algorithms); and 3) build the geomodel. The figure suggests the process is linear, while in reality, there are more feed back loops, multiple iterations at sub task level, and testing and validation at smaller scales.



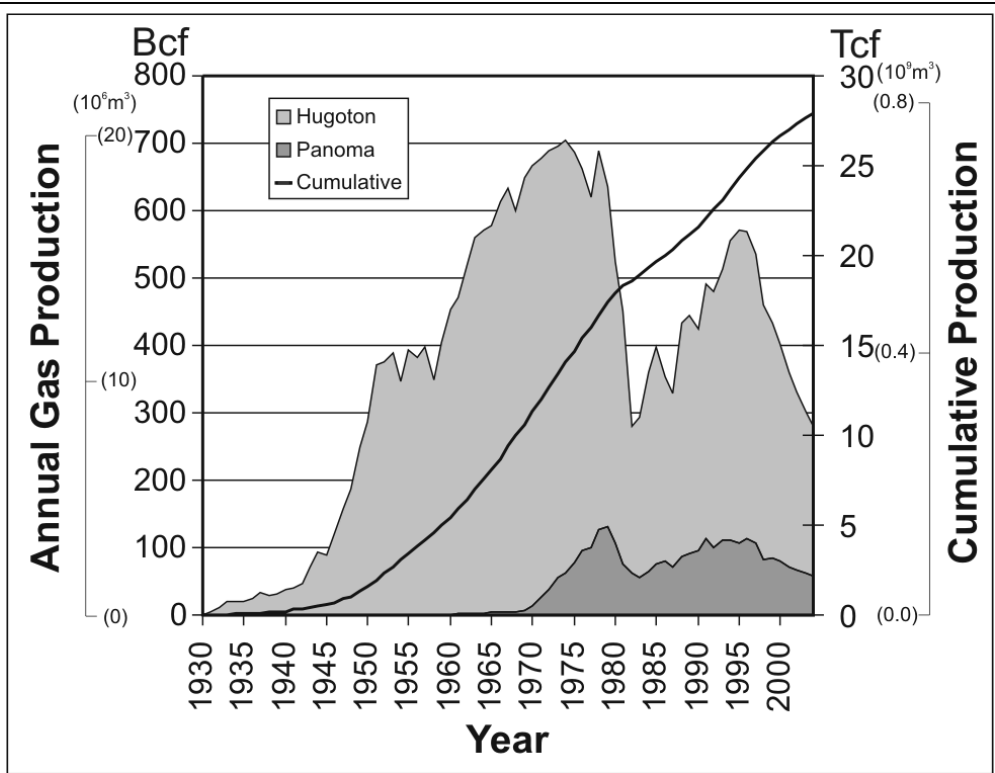


**Figure 1.3.** Gas production from the Wolfcampian (Hugoton and Panoma fields) in the Kansas portion of the study area through 2004. The Oklahoma portion of the study area produced 7 tcf (198 billion  $\text{m}^3$ ) Wolfcampian gas in the same time period that 27 tcf (765 billion  $\text{m}^3$ ) was produced in Kansas. The spike in production beginning in the early 1980's was due to infill drilling the Hugoton field in Kansas.

SYSTEM	SERIES	GROUP	Kansas fields	Oklahoma field
Permian	Leonardian	Sumner		
	Wolfcampian	Chase	Hugoton-Panoma	Guymon-Hugoton
		Council Grove	Byerly Bradshaw	
Pennsylvanian	Virgilian	Admire		
		Wabaunsee	Greenwood	
		Shawnee		

**Figure 1.4.** Stratigraphic column, Hugoton field area with the names of gas fields in Kansas and Oklahoma adjacent to the intervals from which they produce (compiled from Zeller, 1968; Pippin, 1970; Baars et al., 1994; Sawin et al., 2006). The combined Hugoton and Panoma fields in Kansas and the Guymon-Hugoton field in Oklahoma are lumped as “Hugoton” in this paper.

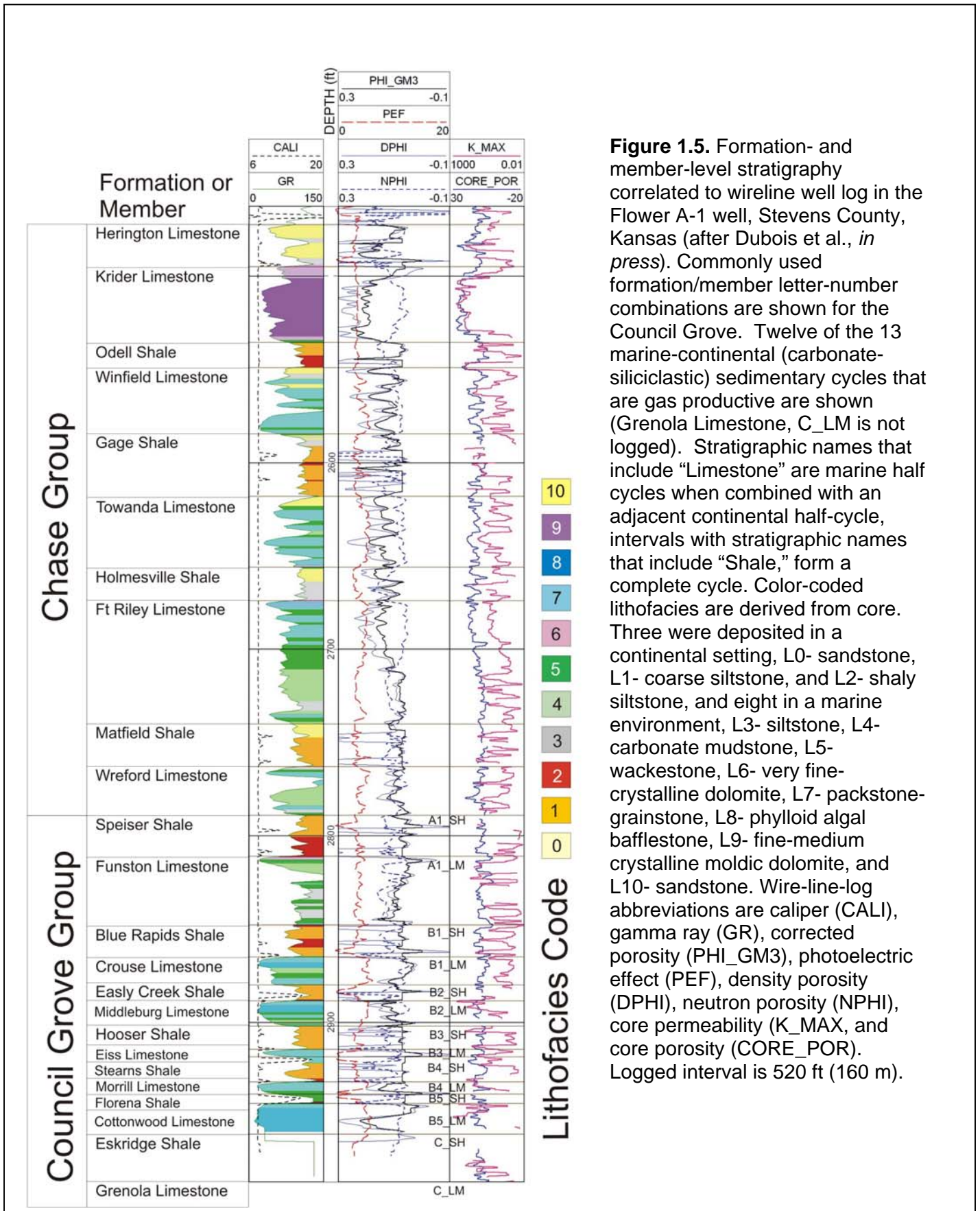


**Figure 1.5.** Formation- and member-level stratigraphy correlated to wireline well log in the Flower A-1 well, Stevens County, Kansas (after Dubois et al., *in press*). Commonly used formation/member letter-number combinations are shown for the Council Grove. Twelve of the 13 marine-continental (carbonate-siliciclastic) sedimentary cycles that are gas productive are shown (Grenola Limestone, C\_LM is not logged). Stratigraphic names that include “Limestone” are marine half cycles when combined with an adjacent continental half-cycle, intervals with stratigraphic names that include “Shale,” form a complete cycle. Color-coded lithofacies are derived from core. Three were deposited in a continental setting, L0- sandstone, L1- coarse siltstone, and L2- shaly siltstone, and eight in a marine environment, L3- siltstone, L4- carbonate mudstone, L5- wackestone, L6- very fine-crystalline dolomite, L7- packstone-grainstone, L8- phylloid algal bafflestone, L9- fine-medium crystalline moldic dolomite, and L10- sandstone. Wire-line-log abbreviations are caliper (CALI), gamma ray (GR), corrected porosity (PHI\_GM3), photoelectric effect (PEF), density porosity (DPHI), neutron porosity (NPHI), core permeability (K\_MAX, and core porosity (CORE\_POR). Logged interval is 520 ft (160 m).